Journal of Power Sources 195 (2010) 2478–2487

Contents lists available at ScienceDirect

Journal of Power Sources

journal homepage: www.elsevier.com/locate/jpowsour

Relevance of the synthesis route of Se-modified Ru/C as methanol tolerant electrocatalysts for the oxygen reduction reaction

M. Montiel[a], S. García-Rodríguez[c], P. Hernández-Fernández[a], R. Díaz[b], S. Rojas[c], J.L. Gª Fierro[c], E. Fatás[a], P. Ocón[a,*]

[a] Departamento de Química Física Aplicada (CII), Universidad Autónoma de Madrid, Madrid, Spain
[b] Departamento de Física Aplicada (CXII), Universidad Autónoma de Madrid, Madrid, Spain
[c] Instituto de Catálisis y Petroleoquímica, CSIC, C/Marie Curie 2, 8049 Madrid, Spain

ARTICLE INFO

Article history:
Received 9 July 2009
Received in revised form 26 October 2009
Accepted 18 November 2009
Available online 27 November 2009

Keywords:
Ruthenium–selenium nanoparticles
Microscopy
X-ray diffraction
X-ray photoelectronic spectroscopy
Oxygen reduction reaction
Methanol tolerance

ABSTRACT

A series of Se-modified Ru/C (Se–Ru/C) samples were prepared from a carbon-supported ruthenium precursor. Selenium was incorporated by two different methods; in the first case, Se was incorporated by treating the Ru/C precursor in a selenious acid solution followed by reduction in H_2 atmosphere. In the second case, Se was incorporated to Ru/C by means of thermal treatment in a selenium atmosphere. The samples thus obtained were characterized by different techniques: X-ray diffraction, energy dispersive X-ray spectroscopy, transmission electron microscopy and X-ray photoelectron spectroscopy. A detailed study has been made of the structural properties and chemical composition of the different Se–Ru/C samples. Microscopy results reveal that Se is incorporated homogeneously, being preferentially located on the surface of the Ru atoms. These results agree well with XRD and XPS data. The incorporation of Se in the lattice results in the formation of $RuSe_2$ only if RuO_2 already exists. On the contrary, if Ru is in its metallic form, Se remains as an amorphous layer located on the surface of the Ru particles. The performance of the catalysts on the oxygen reduction reaction was evaluated either in the absence and presence of methanol. Se-containing samples develop more active and methanol tolerant catalysts, particularly when Se is located on the surface of the Ru particles.

1. Introduction

In recent years, vast amounts of resources have been invested in fuel cell technology. Among the yet-to-be-resolved issues, the design of noble-metal-free electrocatalysts with high ORR activity and methanol tolerance is paramount for the commercialization of direct methanol fuel cells (DMFCs) [1–3]. Ruthenium-based chalcogenides have been proposed as potential candidates to fulfill the requirements of methanol tolerant ORR electrocatalysts [4–8]. Electrochemical investigations have proven that the presence of Se strongly enhances the catalytic activity of Ru in the ORR by preventing the formation of ruthenium oxides [9–11]. Nevertheless, for the purpose of a successful commercialization of Ru-based DMFCs, a further improvement is required in the mass specific activity of these catalysts. Prior papers have reported the potential to further increase the oxygen reduction activity of Se_x–Ru-based electrocatalysts, while maintaining their higher methanol tolerance [6,12].

Se_x–Ru catalysts for the ORR were disclosed in 1988 by Chatzitheodorou [13]. Since then, the preparation of these catalysts via thermolysis has been substantially improved [14–16]. Furthermore, other methods have been reported on their preparation, including precipitation [17,18], reduction [19], impregnation [15], colloidal [20] and reverse micelles methods [21]. The structural characterization of the active material revealed the existence of a Ru-core decorated with a Se-containing shell of complex structure [22,23]. It was established that the presence of Se is the decisive factor for improving catalytic activity and stability compared to unmodified Ru nanoparticles.

Particle aggregation during the synthesis of the Se-modified Ru samples, along with the development of a shell of amorphous Se-containing species, results in samples lacking catalytic activity. Thermal annealing steps during the synthesis of the samples usually results in a more active catalyst due to the reduction of the thickness of the amorphous Se shell; however, particle aggregation is not avoided. Therefore, for this type of solids, batch-to-batch reproducibility is poor. As reported by Hilgendorff et al., the formation of Ru nanoparticles and the subsequent modification with Se must be optimized separately [15]. According to the Bönnemann synthesis route [24], highly dispersed Ru on a carbon black support can be obtained by reducing Ru-salts in solution followed by depositing the colloidal Ru particles onto carbon black (e.g., Vulcan XC-72R). The resultant Se_x–Ru catalyst obtained by addition of Se to

* Corresponding author. Tel.: +34 91 497 2435; fax: +34 91 497 4785.
E-mail address: pilar.ocon@uam.es (P. Ocón).

0378-7753/$ – see front matter.
doi:10.1016/j.jpowsour.2009.11.080

Ru/C recorded a significantly higher activity due to the improved dispersion of the catalytically active particles [15]. Furthermore, all these preparation techniques lead to a product in which Se is firmly bound to Ru with thermal stability up to 850 °C under inert conditions [23].

On the other hand, it was shown that the surface concentration of Se in the catalyst does not increase linearly with the increasing concentration of the H_2SeO_3 solution used in the adsorption step, suggesting that the amount of Se deposited on the surface of the solid could be governed by specific adsorption equilibriums.

In agreement with Zehl et al. [25], the performance of Se–Ru in the ORR is related to the existence of an optimum concentration of Se on the Ru surface. At such a concentration value, a particular chemical structure favourable for the ORR is generated. Above such Se concentration, the catalytic activity of the samples in the ORR decreases. This behaviour could be explained by the formation of catalytically inactive species on the surface of the Ru particles, thus leading to a drop in activity. A given degree of coverage by Se appears to be optimal for designing very active ORR catalysts. In addition, the partial formation of the inactive $RuSe_2$ phase might also take place. Other important parameters for defining the optimum Ru:Se ratio are size and surface structure of the Ru particles.

In this work, we have used two homemade carbon-supported ruthenium samples; the first one was used as prepared and the second one was subjected to thermal treatment at 300 °C in hydrogen, being identified as Ru/C and Ru/C-300, respectively. Both samples have been modified with selenium by two different routes: the first one, as described by Hilgendorff et al. [15], consists in incorporating selenium via the treatment of carbon-supported ruthenium (Ru/C-300) with an aqueous solution of H_2SeO_3 and subsequent reduction at 300 °C under H_2 flow. These latter samples have been used as reference materials. The second route (annealing route) involves the treatment of carbon-supported ruthenium (Ru/C or Ru/C-300) with selenium vapour at low pressure.

The performance of the samples in the oxygen reduction reaction (ORR) has been tested by the thin film rotating disk electrode method. Results show the importance of the presence of Se and its actual nature in the electrode.

Irrespectively of the synthesis method, Se remains as an amorphous layer on the surface of Ru particles. Se incorporation to the Ru lattice is possible only through RuO_2 species, yielding $RuSe_2$. The presence of Se increases the population of Ru^0 species in the samples, resulting in more active catalysts for the oxygen reduction reaction.

2. Experimental

2.1. Synthesis of ruthenium catalysts

Ru-based catalysts were prepared via the colloidal route from $RuCl_3$ (purchased from Johnson Matthey) as metal precursor and carbon Vulcan XC-72R (purchased from Cabot) as carbonaceous support. This method consists in preparing surfactant stabilized colloids in an organic solvent by chemical reduction of metal salt. It has been described by Bönnemann et al. [26]. An adequate amount (0.82 g) of $RuCl_3$ was dissolved in tetrahydrofuran (THF), and a 0.4 M solution of $N(C_8H_{17})_4BEt_3H$ in THF was added dropwise followed by the addition of absolute ethanol (100 mL). The solid was filtered off, washed with ethanol twice and dried in an argon atmosphere. In order to impregnate the carbon substrate with the Ru nanoparticles, the powder obtained was dissolved in THF and added to a suspension of Vulcan carbon (1.6 g) under vigorous stirring. The solvent was removed under reduced pressure, and the residue was washed with H_2O/EtOH (10/90 vol.%) and dried at 70 °C for 8 h. The solid obtained was labelled Ru/C. An aliquot of this sample was subjected to thermal treatment between 25 and 300 °C at a rate of 10 °C min^{-1} under a H_2 flow. The resulting solid was labelled Ru/C-300 (Ru content determined from total reflection X-ray fluorescence analysis: 15 wt%).

Table 1
Preparation method and chemical composition of the catalysts.

Name	Ru precursor	Treatment[a]	Ru %wt.	Se
Annealing route				
A_{100}-$Se_{0.01}$Ru/C	Ru/C	100 (5')	99.5	0.5
A_{150}-$Se_{0.10}$Ru/C	Ru/C	150 (5')	95.4	4.6
A_{150}-$Se_{0.05}$Ru/C-300	Ru/C-300	150 (5')	97.9	2.1
A_{300}-$Se_{0.23}$Ru/C	Ru/C	300 (5')	90.1	9.9
A_{300}-$Se_{0.14}$Ru/C-300	Ru/C-300	300 (5')	94.0	6.0
A_{350}-$Se_{0.11}$Ru/C	A_{300}-$Se_{0.23}$Ru/C	350 (5')	91.9	8.1
A_{350}-$Se_{0.07}$Ru/C-300	A_{300}-$Se_{0.14}$Ru/C-300	350 (5')	96.9	3.1

Name	Ru precursor	[Se][b]	Ru %wt.	Se
Hilgendorff method				
H-$Se_{0.09}$Ru/C-300	Ru/C-300	$6.00\cdot10^{-3}$	95.8	4.2
H-$Se_{0.11}$Ru/C-300	Ru/C-300	$1.25\cdot10^{-2}$	95.0	5.0
H-$Se_{0.27}$Ru/C-300	Ru/C-300	$1.25\cdot10^{-1}$	88.8	11.2

[a] Annealing temperature in °C and time of annealing in (min).
[b] [H_2SeO_3] in mol L^{-1}.

2.2. Synthesis of Se–Ru/C catalysts

In order to synthesize Se-modified Ru/C samples, Se and H_2SeO_3 (purchased from Merck) were used as metal precursors.

2.2.1. Hilgendorff route

For the preparation of the Se-modified samples, 100 mg of Ru/C-300 were transferred to an aqueous solution of H_2SeO_3 and the suspension was treated in an ultrasonic bath for 30 min. The resulting solid was filtered off, dried at 70 °C for 8 h, and exposed to a flow of H_2 at 300 °C. In order to increase the selenium content in the electrocatalysts, the concentration of H_2SeO_3 was increased from 6×10^{-3} to 1.25×10^{-2} M and subsequently to 1.25×10^{-1} M. The samples were labelled as H-Se_xRu/C-300, with x being the actual selenium molar ratio as determined by EDS analysis. See Table 1 for further details.

2.2.2. Annealing route

70 mg of Ru/C or Ru/C-300 and 6 mg of metallic selenium were placed in a quartz tube at a pressure of 1×10^{-6} torr. The ruthenium samples were exposed to a temperature of 300 °C for 5 min under Se atmosphere. Metallic selenium is set at the same temperature as Ru/C or Ru/C-300 during the treatment. Other annealing treatments – 100, 150 and 300 °C for 5 min – were tested in order to modify the composition and nature of the samples. Samples in this series were labelled as A_T-Se_xRu/C and A_T-Se_xRu/C-300, where A stands for annealing route, T denotes the temperature of the thermal treatment and x the actual Se atomic loading as determined by EDS. The conditions of the synthesis of the different samples are shown in Table 1. Samples A_{300}-$Se_{0.14}$Ru/C-300 and A_{300}-$Se_{0.23}$Ru/C were further treated at 350 °C under vacuum.

The morphology and composition of the samples were examined by scanning electron microscopy and EDS in a SEM, Hitachi S-3000N microscope equipped with an energy dispersive X-ray microanalysis unit INCAx-sight (Oxford Inc.).

The X-ray photoelectron spectra (XPS) of the samples were acquired with a VG Escalab 200R spectrometer fitted with a Mg Kα ($h\nu$ = 1253.6 eV) 120 W X-ray source. Samples were pressed into small stainless-steel cylinders and then mounted on a sample rod, placed in a pretreatment chamber, and degassed at room temperature and 10^{-5} mbar for 1 h prior to transfer to the analysis chamber.

Residual pressure was maintained below 3.0×10^{-8} mbar. The 50 eV energy regions of the photoelectrons of interest were scanned a number of times to obtain an acceptable signal-to-noise ratio. Intensities were estimated by calculating the integral of each peak, determined by subtraction of the Shirley-type background and fitting of the experimental curve to a combination of Lorentzian and Gaussian lines of variable proportions. Accurate binding energies (±0.2 eV) were determined by referencing to the C 1s peak at 284.6 eV.

The X-ray diffraction patterns of the samples were collected on a Seifert 3000 powder diffractometer. Scans at 0.04° s^{-1} with a mean time per step of 20 s were recorded for 2θ values between 10° and 90°.

Transmission electron microscopy, high resolution transmission electron microscopy (HRTEM) and high angle annular dark field scanning transmission electron microscopy (HAADF-STEM) images were taken with a 200 kV JEOL JEM-2100F microscope, coupled to an annular dark field detector and equipped with an INCAx-Sight (Oxford Inc.) energy dispersive X-ray spectrometer (EDS). Energy spectra were analyzed with the Microanalysis INCA-EnergyTEM Suite v18.4.11 software package. Energy lines at 2.559 and 1.379 keV corresponding, respectively, to Ru–L and Se–L edges were used for quantification, according to a Cliff–Lorimer routine using the *k* factors included in the software package. Specimens for TEM analyses were prepared by dispersing the powder samples in ethanol. One drop of the resulting suspension was placed on a holey carbon film supported by a copper grid.

The synthesized Se–Ru/C samples have been tested as electrocatalysts for the oxygen reduction reaction (ORR). Their performance was compared to that of Ru/C-300 and a commercial (Johnson Matthey) 40 wt% Pt/C.

Rotating disk electrode (RDE) studies were carried out at 25 °C in a conventional three-compartment electrochemical glass cell. A glassy carbon rotating disk electrode (0.071 cm^2, GC-Typ zu628) was used as a substrate for the catalyst. Prior to each test, the electrode was polished with alumina 0.05 μm to obtain a mirror finish, being then rinsed with triple-distilled water in an ultrasonic bath. A mercury/mercury sulphate electrode and a gold plate were used as the reference and the counter electrodes. All potentials are referred to the reversible hydrogen electrode (RHE).

The samples under study were deposited onto the working electrode by means of an ink: 1 mg of the electrocatalyst, 100 μL of 0.2 wt% of Nafion (alcoholic solution), and 100 μL of Milli-Q water were dispersed in an ultrasonic bath for 45 min, obtaining a homogenous ink. 5 μL of the ink were dropped onto the electrode and dried at room temperature for 15 min resulting in a homogenous coating. A 0.5 M H_2SO_4 (Merck) was used as the electrolyte. All solutions were prepared with Milli-Q water.

Electrochemical measurements were taken with a computer-controlled potentiostat/galvanostat EG&G 273A. The electrode rotation speed was regulated by a Metrohm 628-10 unit. The rotation rate was 1500 rpm.

Cyclic voltammetry (CV) experiments were conducted to clean and activate the electrode surface. Prior to each CV measurement, the electrolyte was purged with nitrogen (Air Liquide) for 30 min to deaerate the system. The samples were cycled at 100 mV s^{-1} between −0.05 and 0.85 V until reproducible voltammograms were obtained.

Linear sweep voltammetry (LSV) was used for the study of the oxygen reduction reaction (ORR) both in the presence and in the absence of methanol. The electrolyte was saturated with high purity oxygen (Air Liquide) for 20 min. The polarization curves were obtained at 2500 rpm at a scan rate of 5 mV s^{-1} between 0.05 and 0.85 V at room temperature.

Current–time experiments were also used for the study of the oxygen reduction reaction (ORR) in the presence of methanol. The electrolyte was saturated with high purity oxygen (Air Liquide) for 20 min. The curves were recorded at 0.6 V vs. RHE at room temperature during 90 min.

For the evaluation of the performance of selected catalysts in DMFC, the membrane electrode assembly (MEA) was manufactured as follows. The anode catalyst was a commercial PtRu/C sample (Johnson Matthey, Pt 20 wt%) whereas the cathode catalyst was H-$Se_{0.11}$Ru/C-300. The Pt and Ru loading in the anode and cathode, respectively, was 1.0 mg cm^{-2}_{MEA}. The effective area of the membranes was 4 cm^2. Prior to assembly the membranes were dried at 60 °C for 10 min. A three-layered structure was used to prepare the MEA. Teflon-treated carbon cloth with a microporous layer (GDL LT1200W, E-TEK) was used as the backing and gas diffusion layer. The catalyst layer was sprayed on the microporous layer of carbon cloth by means of an ink. Typically, the ink was formed by isopropanol (Merck), Milli-Q water, Nafion solution (5 wt%, Aldrich) and powders of catalyst. Nafion content in the ink was 45 wt%. The suspension was dispersed in an ultrasonic bath for 45 min resulting in a homogenous coating. Once the ink was sprayed onto the carbon cloth, the MEA was obtained by hot pressing the anode–membrane–cathode assembly at 100 °C and residual press for 3 min. The DMFC was assembled by mounting the MEA into a 5 cm^2 single cell (Electrochem. Inc.).

After fabrication, each MEA was tested using an Arbin Instruments fuel cell test system by feeding 2 M methanol at a flow rate of 5 mL min^{-1} in the anode side, and oxygen using a constant flow rate of 400 mL min^{-1} and backpressure of 3 bar in the cathode side. Operating cell temperature and fuel and oxidant supply temperature of 90 °C was used in the current study.

3. Results and discussion

The selenization of carbon-supported ruthenium nanoparticles is considered to be the crucial preparation step for defining the morphology and final properties of Se-modified Ru/C samples. In addition, the amount of Se used in this step informs the nature of the samples, particularly at the surface level of the samples.

As described in Section 2, the incorporation of Se has been carried out using two different carbon-supported ruthenium precursors, Ru/C and Ru/C-300, and two different methods, Hilgendorff and annealing routes. The samples obtained by the Hilgendorff method were used as standards, and those obtained via annealing were compared against them. The composition and preparation methods of Se–Ru/C samples, both Hilgendorff and annealing routes, are shown in Table 1.

Ru/C and Ru/C-300 samples were annealed at different temperatures in order to increase the amount of Se incorporated. The influence of annealing temperature on the extent of Se incorporation was different for Ru/C than for Ru/C-300. As deduced from the EDS analysis, the amount of Se incorporated is higher on Ru/C than on Ru/C-300. As shown in Table 1, the Se content in the Ru/C doubles that of Ru/C-300.

On the other hand, regarding the samples synthesized via the Hilgendroff method, aliquots of Ru/C-300 were pretreated in an aqueous solution containing H_2SeO_3. The Se concentration was found to increase with the increasing acid concentration; recording a maximum value of Se (Ru:Se 1:0.27) for 1.25×10^{-1} M H_2SeO_3 as shown in Table 1. This behavior has been observed by other authors [25].

Fig. 1a shows the X-ray diffraction patterns of Ru/C and Ru/C-300. The diffractogram of Ru/C displays a single crystalline phase ascribed to RuO_2 (pdf #04-009-7842), whereas the diffractogram of Ru/C-300 displays reflections ascribed to the h.c.p. phase of metallic ruthenium (pdf #00-006-0663) in line with previous results [11,15].

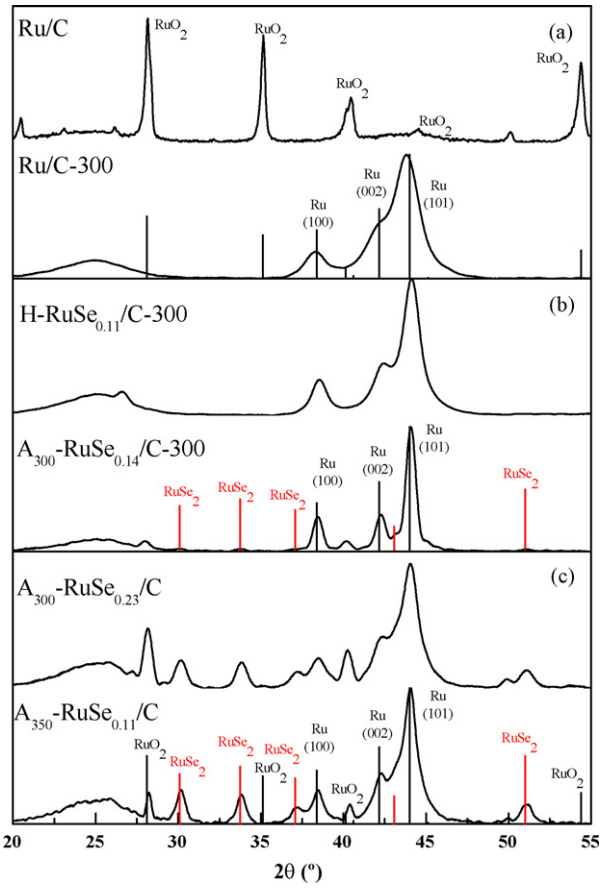

Fig. 1. X-ray diffraction pattern of representative samples: (a) Ru/C and Ru/C-300; (b) H-$Se_{0.11}$Ru/C-300 and A_{300}-$Se_{0.14}$Ru/C-300; (c) A_{300}-$Se_{0.23}$Ru/C and A_{350}-$Se_{0.11}$Ru/C.

Fig. 1b compares representative diffractograms of samples of similar composition prepared from Ru/C-300 obtained via the Hilgendorff and annealing routes, H-$Se_{0.11}$Ru/C-300 and A_{300}-$Se_{0.14}$Ru/C-300, respectively. Reflections ascribed to the Ru h.c.p. phase are the most intense ones observed in either diffractogram. The diffractogram of A_{300}-$Se_{0.14}$Ru/C-300 also depicts faint diffraction lines at 30.1°, 33.7° and 37.1°, suggesting the presence of $RuSe_2$ traces. Although weak, diffraction lines at 28.1° and 40.1°, ascribed to RuO_2, are also visible. Se addition to Ru/C-300 results in a shifting of the Ru^0 diffraction peaks to higher 2θ values. In agreement with Vegard's law, this shifting would correspond to a contraction of the Ru lattice in line with the incorporation of Se into this lattice. Moreover, the lattice parameters (see Table 2) of the Se-modified Ru/C-300 samples are smaller than those of Ru/C-300, 2.705 Å vs. 2.714 Å. This trend is observed for all A_T-Se_xRu/C-300 samples, irrespectively of the annealing as depicted in Table 2. This in turn indicates that such annealing treatment is not ultimately responsible for the variation in the lattice parameter and that such variation accounts solely for the incorporation of Se into the Ru lattice. Remarkably, the value of the lattice parameter is not affected by the actual amount of Se in the sample; a constant value of 2.05 Å (a-axis) is found for A_T-Se_xRu/C-300 samples. This would indicate that only a certain fraction of Se is actually incorporated into the Ru lattice. Samples prepared via the Hilgendorff procedure were also analyzed by XRD (Fig. 1b) and EDS. In line with the results deduced for the annealed samples, reflections ascribed to isolated Se, RuO_2 or $RuSe_2$ phases are not observed. Unlike the A_T-$RuSe_x$/C-300 counterparts, the lattice parameter value recorded for the H-Se_xRu/C-300 samples varied with the amount of Se incorporated; in fact, the higher the amount of Se, the lower the value of the lattice parameter.

Table 2
Structural parameters of the samples.

Sample	T/°C	a[a]/Å	c[a]/Å
Ru[b]		2.706	4.282
Ru/C-300		2.714	4.339
Thermal Treatment			
Ru/C			
A_{100}-$Se_{0.01}$Ru/C	100		
A_{150}-$Se_{0.10}$Ru/C	150		
A_{300}-$Se_{0.23}$Ru/C	300	2.703	4.291
A_{350}-$Se_{0.11}$Ru/C	350 (vacuum)	2.703	4.291
Ru/C-300			
A_{150}-$Se_{0.05}$Ru/C-300	150	2.705	4.266
A_{300}-$Se_{0.14}$Ru/C-300	300	2.705	4.266
A_{350}-$Se_{0.07}$Ru/C-300	350 (vacuum)	2.705	4.266
Hilgendorff method			
H-$Se_{0.09}$Ru/C-300		2.700	4.290
H-$Se_{0.11}$Ru/C-300		2.696	4.314
H-$Se_{0.27}$Ru/C-300		2.691	4.338

[a] Lattice parameters for metallic Ru phase.
[b] pdf #00-006-0663.

As discussed above, the diffractograms of the samples derived from Ru/C-300 show no evidence of isolated Se crystalline phases, with their presence being deduced only by the variations observed on the lattice parameter values. Nevertheless, the presence of an amorphous layer of Se is corroborated by STEM-EDS and XPS analyses, as discussed below.

The samples obtained from Ru/C were annealed at 100, 150 and 300 °C. The diffractograms recorded for A_{100}-$Se_{0.01}$Ru/C and A_{150}-$Se_{0.1}$Ru/C recorded similar diffraction patterns as Ru/C (diffractograms not shown). Reflections ascribed to Se phases are not detected in those diffractograms; however, selenium was detected by EDS analysis. Noticeably, the diffractogram of A_{300}-$Se_{0.23}$Ru/C, see Fig. 1c, displays several crystalline phases: Ru^0, RuO_2 and $RuSe_2$. The lattice parameters of the Ru^0 phase reveal a shrinking of the Ru lattice probably due to the incorporation of Se. In line with the observation for the annealed samples prepared with Ru/C-300, the actual value of the lattice parameter was found to be independent of the actual Se loading, see Table 2. In both samples, diffraction lines from $RuSe_2$ and RuO_2 phases are observed. The main difference between Ru/C and Ru/C-300 series is that $RuSe_2$ and RuO_2 are the predominant crystalline phases in the Ru/C series.

Transmission electron micrographs of H-$Se_{0.11}$Ru/C-300, A_{300}-$Se_{0.14}$Ru/C-300 and A_{300}-$Se_{0.23}$Ru/C are shown in Fig. 2. It is seen that a substantial part of the solids was deposited on the carbon surface in the form of well-dispersed nanoparticles, and the particle distribution is similar for both samples. TEM analysis revealed the presence of nanoparticle agglomerates for both samples, which also agrees well with literature findings [12,27–29]. The mean particle diameter calculated from a population of around 450 particles is 3.5, 4.1 and 5.5 nm, respectively, for H-$Se_{0.11}$Ru/C-300, A_{300}-$Se_{0.14}$Ru/C-300, and A_{300}-$Se_{0.23}$Ru/C.

Fig. 3 shows a HAADF image of H-$Se_{0.11}$Ru/C-300. EDS analyses of the several regions indicated in the figure were also collected. Two types of regions are observed. Regions 1 and 2 correspond to well-dispersed particles displaying a Se content of ca. 18 at%. On the other hand, in regions 3 and 4 particles tend to agglomerate and Se content is ca. 9 at%. Fig. 4a–d shows EDS mappings of selected regions of sample A_{300}-$Se_{0.14}$Ru/C-300 showing a homogenous distribution of Ru and Se in the sample. By focusing the beam on the space between the particles, only the energy lines of C-Kα1 are observed, confirming that Se is deposited on Ru.

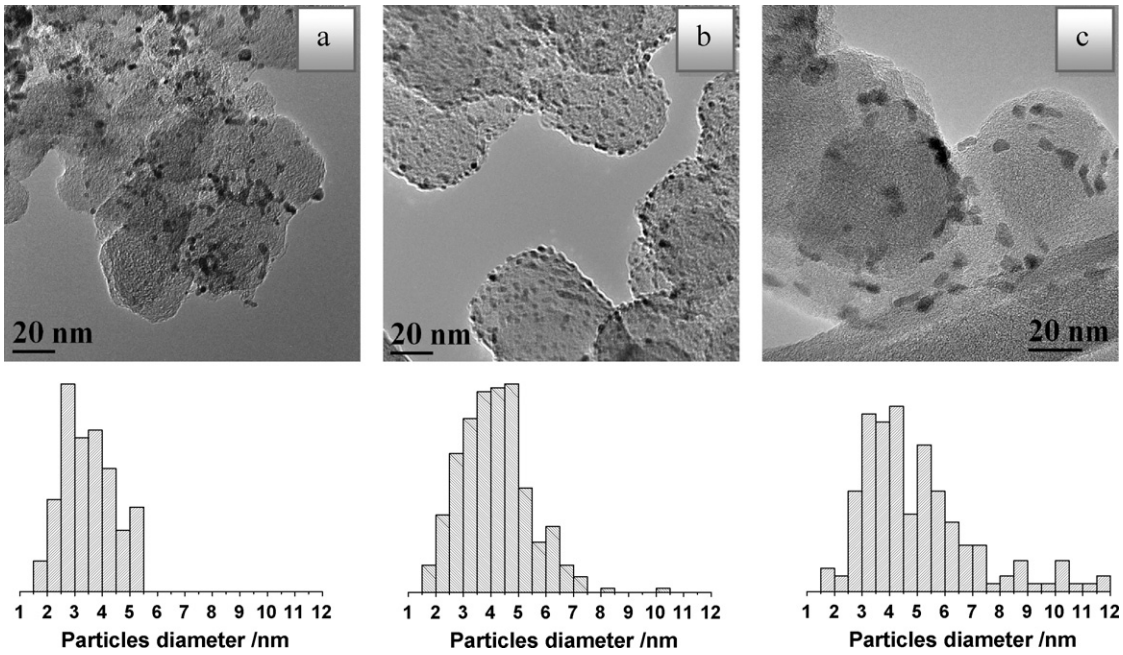

Fig. 2. Representative TEM images of H-$Se_{0.11}$Ru/C-300 (a), A_{300}-$Se_{0.14}$Ru/C-300 (b) and A_{300}-$Se_{0.23}$Ru/C (c) samples and their corresponding particle size distribution histograms.

Although not shown, similar results were found for H-$Se_{0.11}$Ru/C-300. In fact, by comparing two HAADF images recorded under different experimental conditions it is possible to discriminate the atomic distribution of individual particles [30,31]. Thus, Fig. 5a and b shows two STEM-ADF micrographs of an individual particle of H-$Se_{0.11}$Ru/C-300 acquired under different collection angles. Operating in this mode, the signal comes from the collection of Rutherford-scattered electrons. This detector has an annular shape and collects the electrons between an inner and an outer angle, which can be set in the microscope. Contrast in the STEM-ADF images is a function of the atomic number ($\sim Z^2$), thickness ($\sim t$) and inner collection angle. The higher the inner collection angle is, the higher the weight of the Z contrast. The normalized intensity profile of the particle for an inner collection angle of 59.5 and 148.9 mrad is shown in Fig. 5c. When recorded at 148.9 mrad the intensity profile line is sharper (Fig. 5c), suggesting a preferential location of the element of the lower Z value, i.e., Se, on the surface of the particles.

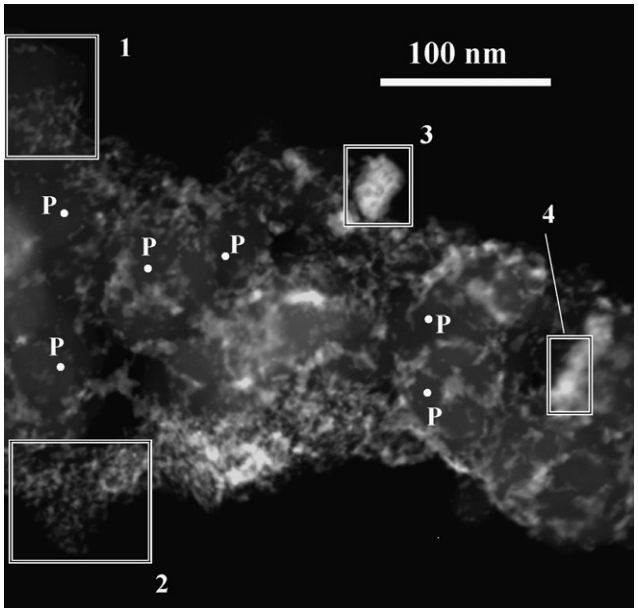

Fig. 3. HAADF-STEM image of H-$Se_{0.11}$Ru/C-300. The atomic composition of selected regions (squared) 1–4 was analyzed by EDS. Point compositional analyses of the carbon support were recorded on P-labelled spots.

Fig. 6a shows an HAADF-STEM image of an individual particle representative of the Se–Ru bimetallic particles found in sample A_{300}-$Se_{0.23}$Ru/C. An EDS profile of this particle is also shown in the figure. Ru and Se atoms are homogeneously distributed in the particle. Quantification of the sum spectrum indicates that the atomic composition of this particle is 63 and 37 at% for Ru and Se, respectively, in good agreement with the stoichiometry of $RuSe_2$ particles observed in the XRD analysis. Although not shown, a number of Se-free particles are also observed, in line with the presence of RuO_2 as observed in the diffractogram of this sample, see Fig. 1c.

Fig. 6b shows a HRTEM image of sample A_{300}-$Se_{0.23}$Ru/C. The inset to the figure depicts an electron diffraction diagram obtained by a fast Fourier transform (FFT) of the selected area in Fig. 5a. The orientation of the particle is close to the [1 0 0] zone axis. The particle displays a pyrite-like cubic structure as expected for the $RuSe_2$ phase.

All in all, microscopy results reveal that Se is incorporated homogenously on the samples of the Ru/C-300 series, being located preferentially on the surface of the Ru atoms. However, Se incorporation on the samples of the Ru/C series results in the formation of $RuSe_2$ crystals rather than an amorphous layer.

X-ray photoelectron spectroscopy (XPS) analysis of the Ru 3p and Ru 3d, C 1s, O 1s, and Se 3d core-levels was performed in order to investigate both the chemical state and surface composition of Ru/C-300, A_{300}-$Se_{0.14}$Ru/C-300 and H-$Se_{0.11}$Ru/C-300 samples. These were also analyzed after being treated in a reducing atmosphere (H_2) to 300 °C in the treatment chamber of the spectrometer. Since the Ru 3d and C 1s energy regions extensively overlap, the Ru 3p core-level spectrum was also recorded. Fig. 7 shows the XPS spectra for Ru $3p_{3/2}$ and Se 3d core-levels of these samples before reduction in H_2. Table 3 compiles the binding energies of core electrons for all the samples.

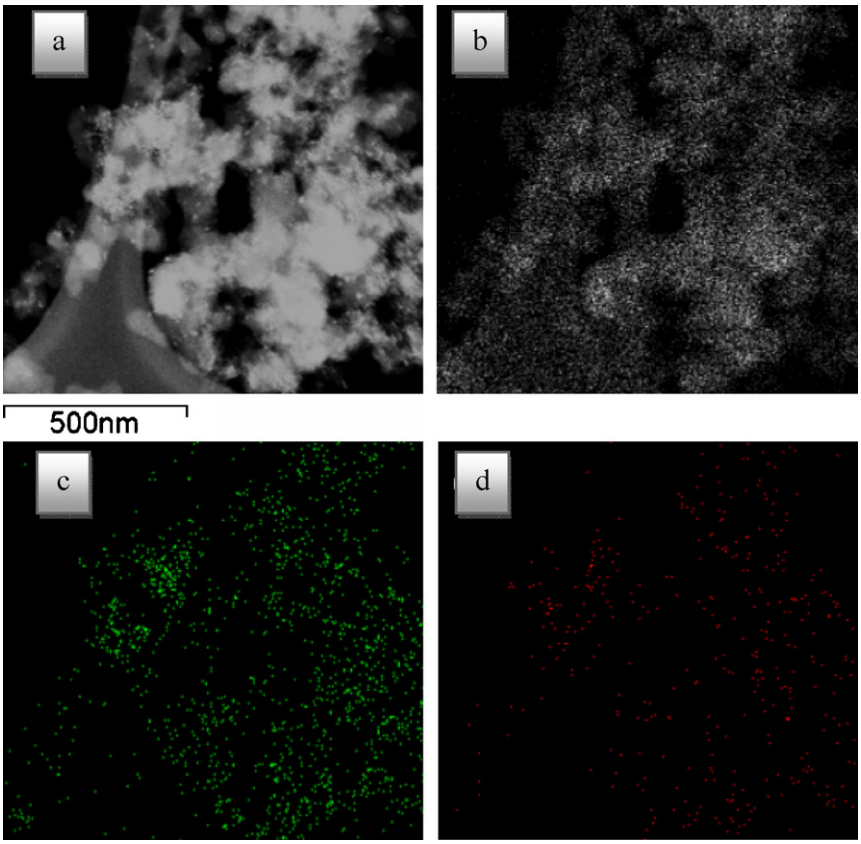

Fig. 4. EDS mapping of A_{300}-$Se_{0.14}$Ru/C-300 sample: (a) HAADF image, (b) C-Kα_1 map, (c) Ru-Lα_1 map and (d) Se-Lα_1 map. Probe size is 1 nm.

The most intense Ru $3p_{3/2}$ peak of the Ru 3p doublet was fitted to two components at about 462.0 and 465.0 eV in the case of A_{300}-$Se_{0.14}$Ru/C-300 and Ru/C-300 samples and about 462.0 and 463.0 eV for H-$Se_{0.11}$Ru/C-300. The peak at lower binding energy could be attributed to the presence of Ru^0 [32,33]. Indeed, the relative abundance of this species is higher in A_{300}-$Se_{0.14}$Ru/C-300 than in H-$Se_{0.11}$Ru/C-300 sample. In addition, the signal at about 465.0 eV is ascribed to upper oxidized ruthenium species, while that close to 463.0 eV could be assigned to Ru(IV) type species [34]. A more precise assignment of this component is difficult since the full weight at high medium value (FWHM) of the peak ascribed to this species is rather large, close to 4 eV.

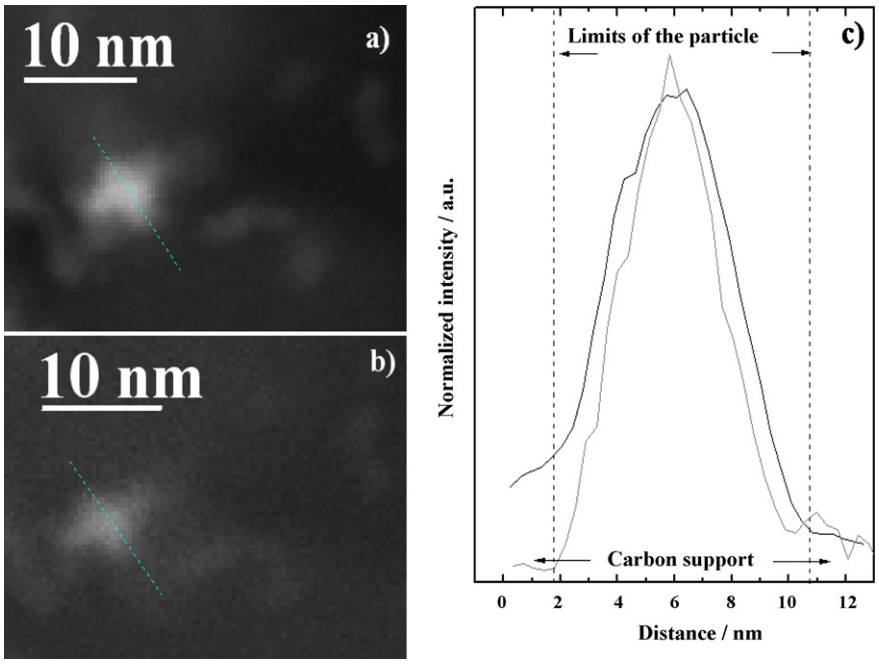

Fig. 5. HAADF images of sample H-$Se_{0.11}$Ru/C-300 recorded with inner collection angles of (a) 59.5 mrad and (b) 148.9 mrad, (c) Normalized intensity linescans; black line 59.5 mrad and grey line 148.9 mrad.

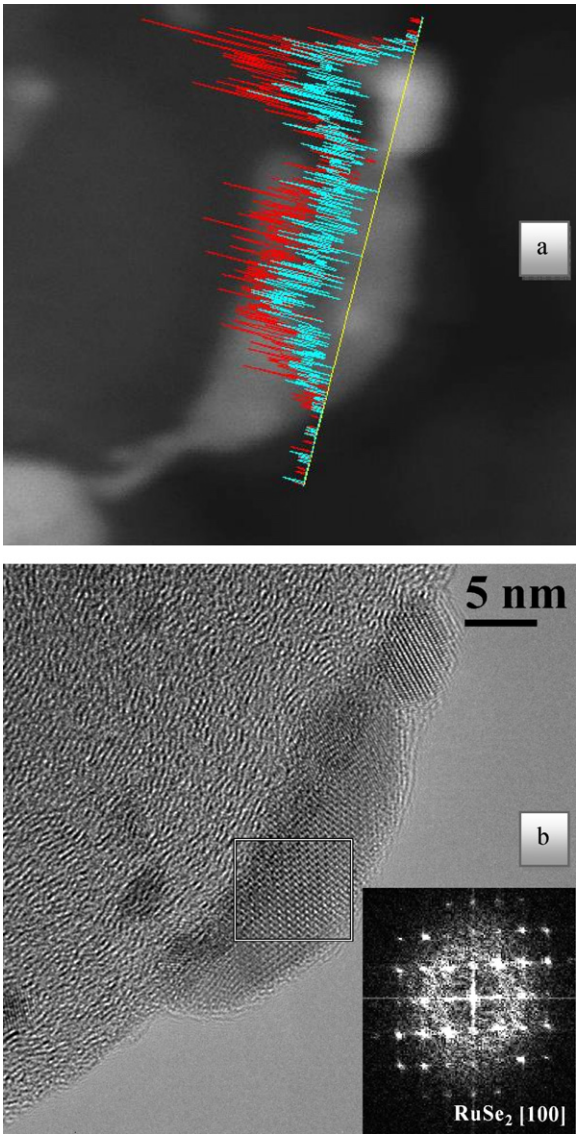

Fig. 6. (a) HAADF image of an individual particle of sample A_{300}-$Se_{0.23}$Ru/C with an EDS linescan distribution of selected energy lines, Se Lα-1 (red) and Ru Lα-1 (blue) (b) high resolution TEM image of the same particle. The inset to the figure is a FFT processed image of the selected area. (For interpretation of the references to color in this figure legend, the reader is referred to the web version of the article.)

Upon in situ H_2-treatment, A_{300}-$Se_{0.14}$Ru/C-300 sample exhibited a binding energy of the Ru $3p_{3/2}$ peak characteristic of Ru^0, indicating a complete reduction of ruthenium on the sample surface. However, the Ru $3p_{3/2}$ spectrum of the sample prepared according to Hilgendorff's methodology revealed two components at similar binding energy and displaying a similar relative abundance as that before H_2 treatment.

On the other hand, the Se 3d spectra of either sample revealed two components at binding energies of 55.3 and 58.9 eV. These binding energies are ascribed to Se^{2-} (or Se^0) and Se^{4+} species, respectively [11,12]. After hydrogen treatment, the complete reduction of oxidized species (Se^{4+}) is observed.

XPS results confirm the presence of Se in all samples. As shown in Table 3, the Se/Ru atomic ratio is higher when observed by XPS (a surface analysis technique) than by EDS. This result is in good agreement with a preferential location of Se on the surface of the Ru atoms, Furthermore, the population of Ru^0 species increases and that of upper Ru oxides decreases in the Se-containing samples.

For further discussion, samples will be divided as a function of the Ru precursors. Scheme 1 depicts the synthesis paths described here and summarizes the main Ru and Se phases detected. XRD data reveal that Ru^0 is the only crystalline species obtained after Se-treatment when using Ru/C-300 as precursor. XPS and microscopy data confirm that Se is actually present in these samples, being located on the surface of the Ru atoms. Remarkably, when synthesized by the annealing route, even if Ru^0 is still the predominant phase, faint RuO_2 or $RuSe_2$ diffraction peaks are visible. This observation could indicate that Se incorporation to the Ru^0 lattice is impeded and only proceeds through RuO_2. It should be stressed that unlike the annealing approach, Hilgendorff synthesis maintains a reduction atmosphere during the synthesis of the Se–Ru particles and this difference can be crucial for the formation of $RuSe_2$ via RuO_2.

To confirm this hypothesis, Ru/C was used as precursor. This Ru precursor comprises RuO_2 phases only (see Fig. 1a and discussion above). No Ru^0 phases are observed for this solid. First, the amount of Se actually incorporated on the A_T-Se_xRu/C solids doubles that of A_T-Se_xRu/C-300 at every temperature studied. Furthermore, XRD and microscopy analyses, see Fig. 1c and Fig. 6a and b, reveal the preferential formation of $RuSe_2$ at the expense of RuO_2. In fact, it can be observed that the disappearance of RuO_2 results in the preferential formation of $RuSe_2$ and only a minor amount of Ru^0 is formed in spite of the severe reduction treatment (H_2, 300 °C) that proved to be sufficient for reducing RuO_2 to Ru^0 in the bare-Ru/C solids.

These results indicate that $RuSe_2$ formation upon Se treatment of Ru-containing samples is favoured when the predominant phase on the parent material is RuO_2 rather than Ru^0. In fact, the formation of $RuSe_2$ from Ru^0 is not straightforward and can only take place through the previous oxidation of Ru^0 to RuO_2.

Finally, the stability of the solids was studied by annealing A_{300}-$Se_{0.23}$Ru/C at 350 °C under vacuum. Fig. 1c shows that the intensity of the reflections ascribed to the RuO_2 phase decreased after the vacuum annealing treatment, while those of the $RuSe_2$ phase remained essentially unchanged. No reflections ascribed to isolated Se crystals are observed. After thermal treatment, the Se/Ru atomic ratio decreases from 0.23 (A_{300}-$Se_{0.23}$Ru/C) to 0.07 (A_{350}-$Se_{0.11}$Ru/C). Furthermore, a clear decrease in the RuO_2 concentration is observed after the vacuum annealing treatment (see Fig. 1c). The disappearance of the RuO_2 phase is not accompanied by the appearance of other Ru species. Therefore, Ru should have been transformed either as RuO_2xH_2O or as RuO_3 phase. The former

Table 3
Binding energies in eV, and atomic percentage (in brackets) of H-$Se_{0.11}$Ru/C-300 and A_{300}-$Se_{0.14}$Ru/C-300 samples from XPS measurements.

Sample	Ru $3p_{3/2}$			Se 3d		Se/Ru at. (XPS)	Se/Ru at. (EDS)
	Ru^{upper}	Ru^{4+}	Ru^0	Se^{4+}	Se^0/Se^{2-}		
Ru/C-300	465.2 (31)		462.0 (69)				
A_{300}-$Se_{0.14}$Ru/C-300	465.2 (6)	–	462.2 (94)	58.9 (38)	55.3 (62)	0.25	0.14
A_{300}-$Se_{0.14}$Ru/C-300 + 300 °C/H_2	–	–	461.8	–	55.0	0.27	
H-$Se_{0.11}$Ru/C-300	–	463.1 (34)	461.6 (66)	58.6 (27)	55.2 (72)	0.14	0.11
H-$Se_{0.11}$Ru/C-300 + 300 °C/H_2	–	463.2 (32)	461.5 (68)	–	55.2	0.17	

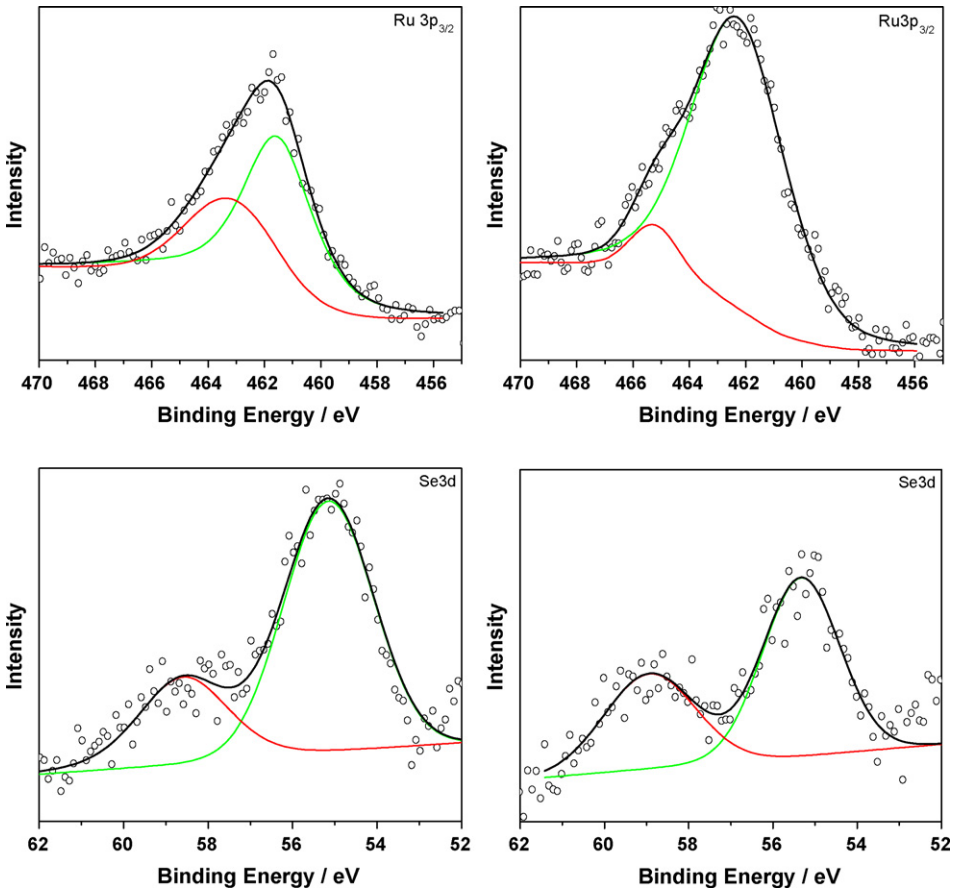

Fig. 7. Ru $3p_{3/2}$ and Se 3d core level spectra of the H-$Se_{0.11}$Ru/C-300 (up) and A_{300}-$Se_{0.14}$Ru/C-300 (down) samples.

species is known to be amorphous [35] showing no diffraction pattern, whereas the latter is unstable in solid phase [36], with neither species showing diffraction peaks.

It is well accepted that samples containing metallic Ru or Se-decorated Ru particles will develop more active cathode electrocatalysts than those containing Ru oxide or $RuSe_2$ phases [10,22]. Results obtained here suggest that by using Ru/C-300 as precursor, the amount of Ru and Se-decorated Ru phase increases in the solids.

The oxygen reduction reaction (ORR) activities of the prepared catalysts were measured by the thin film rotating disk electrode (RDE) technique. The *j*–*E* profiles recorded for $Se_{0.11}$Ru/C-300, A_{300}-$Se_{0.14}$Ru/C-300 and A_{300}-$Se_{0.23}$Ru/C with Ru/C-300 are depicted in Fig. 8. From the figure it can be concluded that the electrochemical reaction operates under mixed kinetic-diffusion control in the potential range between the open circuit voltage (OCV) and 0.5 V, and diffusion limited current is almost reached below 0.5 V. The net reduction current on Ru/C-300 starts at 0.75 V and increases as the potential is scanned from 0.75 to 0.2 V. On the Se-modified catalysts, the onset of the net reduction currents is shifted to more positive values. In sample H-$Se_{0.11}$Ru/C-300, the

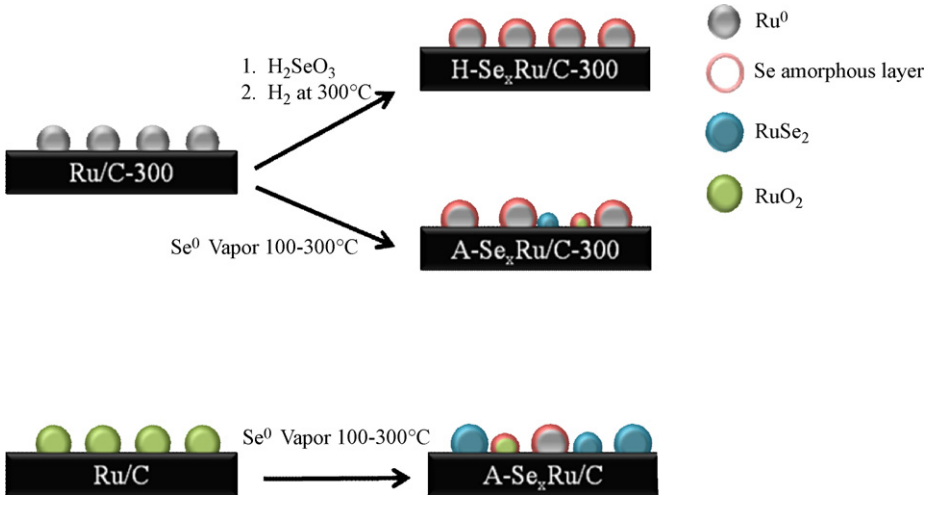

Scheme 1. Illustrative paths of the samples prepared by modifying Ru/C-300 and Ru/C with Se.

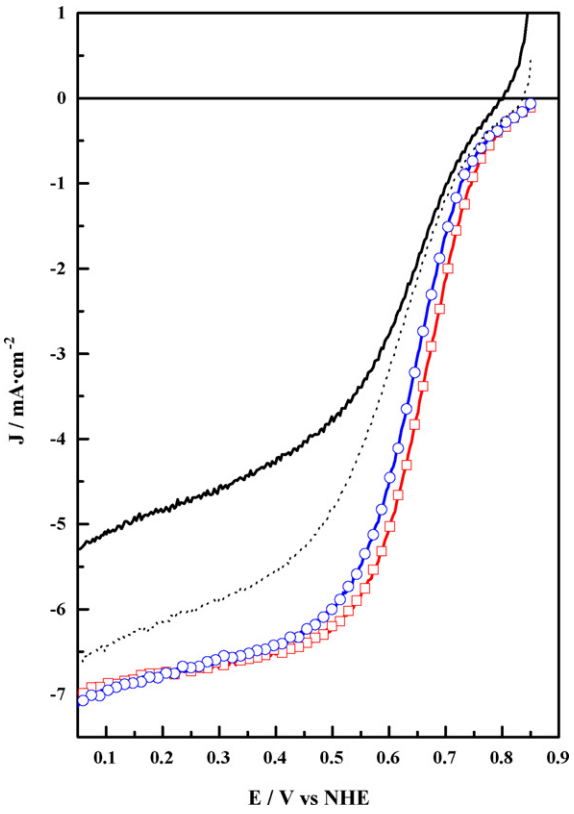

Fig. 8. RDE polarization curves in 0.5 M H_2SO_4 recorded a 2500 rpm for Ru/C-300 (black line), H-$Se_{0.11}$Ru/C-300 (red square), A_{300}-$Se_{0.14}$Ru/C-300 (blue circle), and A_{300}-$Se_{0.23}$Ru/C (dotted line). (For interpretation of the references to color in this figure legend, the reader is referred to the web version of the article.)

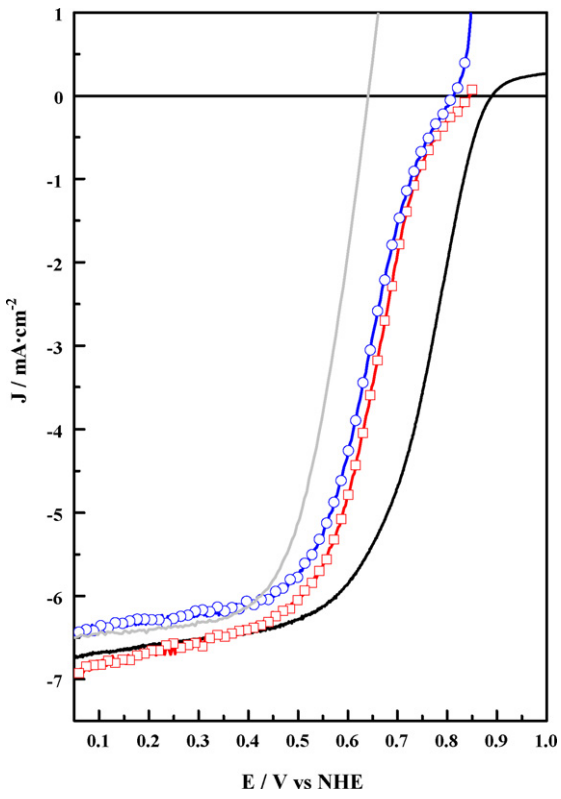

Fig. 9. Current–potential curves for oxygen reduction in 0.5 M H_2SO_4 for Pt/C (black line) and in 0.5 M H_2SO_4 0.1 M MeOH for H-$Se_{0.11}$Ru/C-300 (red squares), A_{300}-$Se_{0.14}$Ru/C-300 (blue circles), and Pt/C (grey line) recorded a 2500 rpm. (For interpretation of the references to color in this figure legend, the reader is referred to the web version of the article.)

onset potential is located at 0.85 V, the most positive value of the series. H-$Se_{0.11}$Ru/C-300 and A_{300}-$Se_{0.14}$Ru/C-300 display similar ORR polarization curves. Higher current densities are found for the Se-modified samples throughout the entire polarization curve. It is known that ruthenium oxide or hydroxide films record poor activity for oxygen reduction [10]. Nevertheless, it is accepted that selenium is able to suppress the formation of inactive RuO_x layers [10,37,38], Although not shown, we have observed this feature by means of cyclic voltammetry measurements in an oxygen-free H_2SO_4 electrolyte. This effect leads to higher catalytic activity in the ORR as compared to Se-free Ru samples. Comparing the precursors, Ru/C-300 provides more active species than Ru/C. In the same way, comparing the preparation methods, the Hilgendorff route leads to a better catalyst than the annealing route (H-$Se_{0.11}$Ru/C-300 vs. A_{300}-$Se_{0.14}$Ru/C-300), probably as a result of the higher amount of Ru exposed (see Se/Ru atomic ratios in Table 3) or due to the presence of $RuSe_2$ in A_{300}-$Se_{0.14}$Ru/C-300. As stated above, the presence of ruthenium oxides produces a decrease in catalytic activity. In the same way, ruthenium selenide ($RuSe_2$) is almost inactive in the oxygen reduction reaction [10,39]. Thus, the poor activity of the sample prepared from Ru/C (A_{300}-$Se_{0.23}$Ru/C), as compared to those prepared on Ru/C-300 is ascribed to the presence of $RuSe_2$. However, its performance is superior to that of Ru/C-300, revealing a certain promotion due to the presence of Se. Nevertheless, the presence of selenium always leads to an improvement over the Se-free sample. Its stabilization effect facilitates oxygen adsorption on the bimetallic catalysts and a better electron transfer between reactants and the catalyst active sites due to the well-documented influence of Se [20,38].

On the other hand, the most relevant feature of Se-modified Ru catalysts is expected from their tolerance to methanol during the ORR. LSV experiments in the presence of 0.1 M CH_3OH have been recorded on samples H-$Se_{0.11}$Ru/C-300 and A_{300}-$Se_{0.14}$Ru/C-300; results are shown in Fig. 9. For the sake of comparison, the activity of commercial Pt/C is also shown. On the Pt/C sample, the ORR starts at potentials around 0.6 V, in agreement with previous results [6]. The net current ascribed to the ORR on the Se-modified samples begins at 0.8 V, that is, both samples display a much higher tolerance to methanol than Pt/C. In fact, neither H-$Se_{0.11}$Ru/C-300 nor A_{300}-$Se_{0.14}$Ru/C-300 seems to be active in the methanol oxidation reaction. The *j*–*E* curve recorded for both samples is very similar, reaching a limiting current value at ca. 0.5 V. Current–time experiments at 0.6 V in the presence of 0.1 M CH_3OH have been recorded

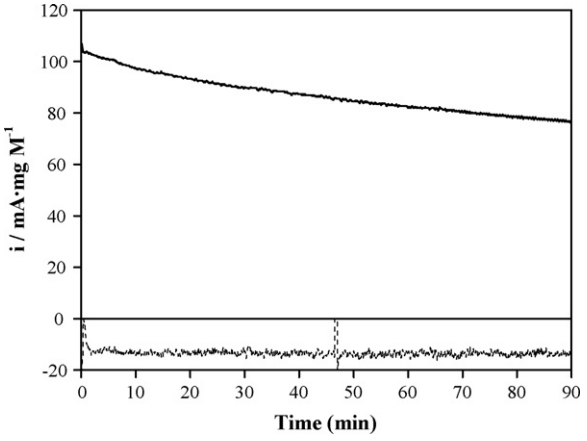

Fig. 10. Current–time curves recorded at 0.6 V.in oxygen saturated 0.5 M H_2SO_4 0.1 M MeOH solutions on Pt/C (black line) and H-$Se_{0.11}$Ru/C-300 (grey dotted line).

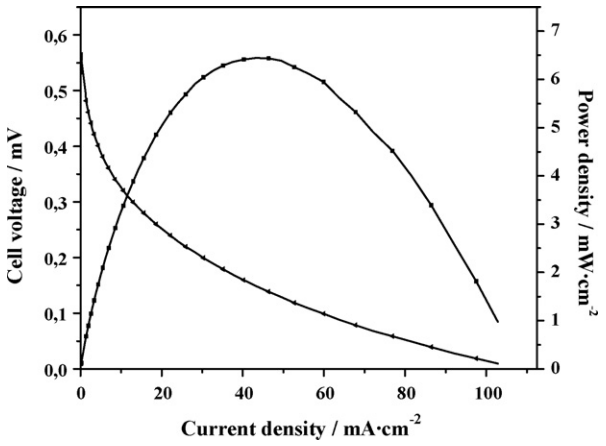

Fig. 11. Polarization and power density curves obtained with catalyst H-$Se_{0.11}$Ru/C-300 recorded at; cathode feed 400 mL min^{-1} of O_2 at 40 psi and anode feed 5 mL min^{-1} of methanol at 5 psi at 90 °C.

on sample H-$Se_{0.11}$Ru/C-300 and Pt/C; results are shown in Fig. 10. These experiments have been carried out using a static electrode. Under these reaction conditions oxygen diffusion to electrode is not favoured as it is in the rotating disk electrode configuration. On the Pt/C sample the net current is positive whereas on H-$Se_{0.11}$Ru/C-300 is negative. That is, the Se-modified Ru sample shows more tolerance to methanol than platinum sample. These results are in good agreement with the results commented previously. The performance of H-$Se_{0.11}$Ru/C-300 has been evaluated in a 5 cm^2 fuel cell. Polarization and power density curves recorded at 90 °C are shown in Fig. 11. The maximum power density value, obtained at is ca. 7 mW cm^{-2}. This power density value, normalized to the actual Ru loading of the electrode, is in line with previous reports for similar RuSe catalysts [40–42] but inferior to Pt-containing catalysts [43].

4. Conclusions

Se incorporation on carbon-supported Ru samples follows different paths depending on the actual nature of the Ru precursor and the synthesis route. If Ru^0 is the predominant phase, Se is incorporated as an amorphous layer located on Ru particles. However, if RuO_2 is the predominant phase, Se incorporation leads to the formation of $RuSe_2$. This latter sample, however, is not active as a catalyst in the oxygen reduction reaction. The presence of Se increases the population of Ru^0 species on the samples. This in turn results in more active catalysts for the oxygen reduction reaction. Furthermore, the tolerance to the presence of methanol during the oxygen reduction reaction is remarkably improved on Se-modified catalysts.

Acknowledgements

The Comisión Interministerial de Ciencia y Tecnología (*CICYT*) project reference CTQ-2007-66547/BQU is acknowledged for its financial support. M. Montiel thanks the CAR for a grant. S. Rojas acknowledges CSIC project 200780I017 for support; S.G. acknowledges I3P Program for a fellowship.

References

[1] L. Zhang, J. Zhang, D.P. Wilkinson, H. Wang, J. Power Sources 156 (2006) 171–182.
[2] D. Chu, R. Jiang, Solid State Ionics 148 (2002) 591–599.
[3] J.-W. Lee, B.N. Popov, J. Solid State Electrochem. 11 (2007) 1355–1364.
[4] N. Alonso-Vante, P. Bogdanoff, H. Tributsch, J. Catal. 190 (2000) 240.
[5] A.K. Shukla, R.K. Raman, Annu. Rev. Mater. Res. 33 (2003) 155–168.
[6] D. Cao, A. Wieckowski, J. Inukai, N. Alonso-Vante, J. Electrochem. Soc. 153 (2006) A869–A874.
[7] L. Colmenares, Z. Jusys, R.J. Behm, J. Phys. Chem. C 111 (2007) 1273–1283.
[8] D.C. Papageorgopoulos, F. Liu, O. Conrad, Electrochim. Acta 52 (2007) 4982–4986.
[9] K. Suárez-Alcántara, O. Solorza-Feria, Electrochim. Acta 53 (2008) 4981–4989.
[10] H. Schulenburg, M. Hilgendorff, I. Dorbandt, J. Radnik, P. Bogdanoff, S. Fiechter, M. Bron, H. Tributsch, J. Power Sources 155 (2006) 47–51.
[11] V. Zaikovskii, K.S. Nagabhushana, V.V. Kriventsov, K.N. Loponov, S.V. Cherepanova, R.I. Kvon, H. Bönnemann, D.I. Kochubey, E.R. Savinova, J. Phys. Chem. B 110 (2006) 6881–6890.
[12] M. Bron, P. Bogdanoff, S. Fiechter, M. Hilgendorff, J. Radnik, I. Dorbandt, H. Schulenburg, H. Tributsch, J. Electroanal. Chem. 517 (2001) 85–94.
[13] G. Chatzitheodorou, Patent DE 38 02 136 A1 (1988), 12.
[14] N. Alonso-Vante, Patent DE 196 44 628 A1 (1996), 6.
[15] M. Hilgendorff, K. Diesner, H. Schulenburg, P. Bogdanoff, M. Bron, S. Fiechter, J. New Mater. Electrochem. Syst. 5 (2002) 71–81.
[16] P. Bogdanoff, S. Fiechter, H. Tributsch, M. Bron, I. Dorbandt, M. Hilgendorff, H. Schulenburg, Patent DE 100 35 841 A1 (2000), 16.
[17] V. Trapp, P.A. Christensen, A. Hamnett, J. Chem. Soc., Faraday Trans. 92 (1996) 4311–4319.
[18] R.W. Reeve, P.A. Christensen, A. Hamnett, S.A. Haydock, S.C. Roy, J. Electrochem. Soc. 145 (1998) 3463–3471.
[19] A. Stephen, U.S. Campbell, Patent 2004/0096728A1 (2004).
[20] H. Tributsch, M. Bron, M. Hilgendorff, H. Schulenburg, I. Dorbandt, V. Eyert, P. Bogdanoff, S. Fiechter, J. Appl. Electrochem. 31 (2001) 739–748.
[21] C.V. Rao, B. Viswanathan, J. Phys. Chem. C 111 (2007) 16538–16543.
[22] S. Fiechter, I. Dorbandt, P. Bogdanoff, G. Zehl, H. Schulenburg, H. Tributsch, M. Bron, J. Radnik, M. Fieber-Erdmann, J. Phys. Chem. C 111 (2007) 477–487.
[23] G. Zehl, I. Dorbandt, G. Schmithals, J. Radnik, K. Wippermann, B. Richter, P. Bogdanoff, S. Fiechter, ECS Trans. 3 (2006) 1261.
[24] H. Bönnemann, K.S. Nagabhuskana, J. New Mater. Electrochem. Syst. 7 (2004) 93.
[25] G. Zehl, P. Bogdanoff, I. Dorbandt, S. Fiechter, K. Wippermann, C. Hartnig, J. Appl. Electrochem. 37 (2007) 1475–1484.
[26] H. Bönnemann, W. Brijoux, R. Brinkmann, E. Dinjus, T. Jouben, B. Korall, Angew. Chem. 103 (1991) 1344–1346.
[27] A.A. Serov, M. Min, G. Chai, S. Han, S. Kang, C. Kwak, J. Power Sources 175 (2008) 175–182.
[28] D. Leveratto, A. Racz, E.R. Savinova, U. Stimming, Fuel Cells 3–4 (2006) 203–207.
[29] C. Cremers, M. Scholz, W. Seliger, A. Racz, W. Knechtel, J. Rittmayr, F. Grafwallner, H. Peller, U. Stimming, Fuel Cells 1 (2007) 21–31.
[30] J. Liu, J. Electron Microsc. 54 (2005) 251–278.
[31] T. Akita, T. Hiroki, S. Tanaka, T. Kojima, M. Kohyama, A. Iwase, F. Hori, Catal. Today 131 (2008) 90–97.
[32] C. Roth, M. Goetz, H. Fuess, J. Appl. Electrochem. 31 (2001) 793–798.
[33] Z. Liu, J.Y. Lee, W. Chen, M. Han, L.M. Gan, Langmuir 20 (2004) 181–187.
[34] M. Montiel, P. Hernández-Fernández, J.L.G. Fierro, S. Rojas, P. Ocón, J. Power Sources 191 (2009) 280–288.
[35] J.P. Zheng, P.J. Cygan, T.R. Jow, J. Electrochem. Soc. 142 (1995) 2699–2703.
[36] D.R. Rolison, P.L. Hagans, K.E. Swider, J.W. Long, Langmuir 15 (1999) 774–779.
[37] P.K. Babu, A. Lewera, J.H. Chung, R. Hunger, W. Jaegermann, N. Alonso-Vante, A. Wieckowski, E. Oldfield, J. Am. Chem. Soc. 129 (2007) 15140–15141.
[38] M. Bron, P. Bogdanoff, S. Fiechter, I. Dorbandt, M. Hilgendorff, H. Schulenburg, H. Tributsch, J. Electroanal. Chem. 500 (2001) 510–517.
[39] Y. Hara, N. Minami, H. Itagaki, Appl. Catal. A: Gen. 340 (2008) 59–66.
[40] H. Cheng, W. Yuan, K. Scott, Fuel Cells 1 (2007) 16–20.
[41] K. Scott, A.K. Shukla, C.L. Jackson, W.R.A. Meuleman, J. Power Sources 126 (2004) 67–75.
[42] H. Cheng, W. Yuan, K. Scott, Electrochim. Acta 52 (2006) 466–473.
[43] P. Hernández-Fernández, S. Rojas, P. Ocón, A. de Frutos, J.M. Figueroa, P. Terreros, M.A. Peña, J.L.G. Fierro, J. Power Sources 177 (2008) 9–16.